frontiers in Chemistry

ORIGINAL RESEARCH
published: 29 March 2022
doi: 10.3389/fchem.2022.870985

Computational Exploration on the Structural and Optical Properties of Gold-Doped Alkaline-Earth Magnesium $AuMg_n$ (n = 2–12) Nanoclusters: DFT Study

Ben-Chao Zhu, Ping-Ji Deng, Jia Guo and Wen-Bin Kang**

School of Public Health, Hubei University of Medicine, Shiyan, China

Using CALYPSO crystal search software, the structural growth mechanism, relative stability, charge transfer, chemical bonding and optical properties of $AuMg_n$ (n = 2–12) nanoclusters were extensively investigated based on DFT. The shape development uncovers two interesting properties of $AuMg_n$ nanoclusters contrasted with other doped Mg-based clusters, in particular, the planar design of $AuMg_3$ and the highly symmetrical cage-like of $AuMg_9$. The relative stability study shows that $AuMg_{10}$ has the robust local stability, followed by $AuMg_9$. In all nanoclusters, the charge is transferred from the Mg atoms to the Au atoms. Chemical bonding properties were confirmed by ELF analysis that Mg-Mg formed covalent bonds in nanoclusters larger than $AuMg_3$. Static polarizability and hyperpolarizability calculations strongly suggest that $AuMg_9$ nanocluster possesses interesting nonlinear optical properties. Boltzmann distribution weighted average IR and Raman spectroscopy studies at room temperature verify that these nanoclusters are identifiable by spectroscopic experiments. Finally, the average bond distance and average nearest neighbor distance were fully investigated.

Keywords: calypso, DFT, AuMgn nanoclusters, optical properties, structural property

OPEN ACCESS

Edited by:
Ambrish Kumar Srivastava, Deen Dayal Upadhyay Gorakhpur University, India

Reviewed by:
Ruby Srivastava, Centre for Cellular and Molecular Biology (CCMB), India
Shamoon Ahmad Siddiqui, Najran University, Saudi Arabia

****Correspondence:***
Ben-Chao Zhu
benchao_zhu@126.com
Wen-Bin Kang
wbkang@hbmu.edu.cn

Specialty section:
This article was submitted to Physical Chemistry and Chemical Physics, a section of the journal Frontiers in Chemistry

Received: *07 February 2022*
Accepted: *04 March 2022*
Published: *29 March 2022*

Citation:
Zhu B-C, Deng P-J, Guo J and Kang W-B (2022) Computational Exploration on the Structural and Optical Properties of Gold-Doped Alkaline-Earth Magnesium $AuMg_n$ (n = 2–12) Nanoclusters: DFT Study. Front. Chem. 10:870985. doi: 10.3389/fchem.2022.870985

INTRODUCTION

Metal nanoclusters have attracted increasing interest from academics in recent years due to their appealing micro patterns and interesting features (Jin et al., 2016; Peng et al., 2018; Tew et al., 2018). For example, Au_n clusters tend to exhibit 2-dimensional structures at small sizes, while medium sizes (n < 15) will transition to 3-dimension (Idrobo et al., 2007; Assadollahzadeh and Schwerdtfeger, 2009; Huang and Wang, 2009). For larger size, the study of Au_{144} cluster is highly worth explaining. It was first reported in 1997 as a critical size for the transformation of Au nanoclusters into nanocrystals and worthy of being researched, but its structure could not be determined at that time (Alvarez et al., 1997), then in 2009 it was precisely predicted by theoretical studies to have a multishell structure (Qian and Jin, 2009), and finally, in 2018 it was experimentally confirmed to have a three-layer metallic core of Au_{12}-Au_{42}-Au_{60} from the inside out (Yan et al., 2018). Researchers have been so persistent in studying them because the physical size of these clusters is comparable to the electron Fermi wavelength and therefore tends to show interesting electronic (Yau et al., 2013), optical properties (Ramakrishna et al., 2008; Jin, 2015) and have important application prospects in the field of medicine and biology (Shang et al., 2011). Because the physical and chemical characteristics of

nanoclusters alter with size throughout the transition to nanocrystals or nanoparticles, nanocluster research will anticipate, at least theoretically, a slew of new materials for the field of nanomaterials science.

A lot of studies on alkaline Earth metal magnesium clusters have been reported, in addition to usual studies of metal nanoclusters like gold, silver, and copper (Köhn et al., 2001; Xia et al., 2016; Zhang et al., 2020; Zhao et al., 2021). This is partly because magnesium-based nanomaterials have an exceptional hydrogen storage capacity compared to ordinary materials (Shao et al., 2012), and therefore, various kinds of Mg-based nanocluster materials, such as $CoMg_n$ (Trivedi and Bandyopadhyay, 2015), $RhMg_n$ (Trivedi and Bandyopadhyay, 2016), ScMg nanocluster (Chen et al., 2020; Lyon, 2021), are worthy of systematic study. Most of these studies were carried out theoretically and gave interesting results by predicting the hydrogen storage properties of nanocluster materials based on Mg. For example, it is shown that $MgScH_{13}$ and $MgScH_{15}$ nanoclusters have, theoretically, ultra-high hydrogen storage capacities of 15.9 wt% (Lyon, 2021) and 17.8 wt% (Chen et al., 2020), respectively. On the other hand, the optical properties of Mg and Mg-based nanoclusters are also very attractive (Belyaev et al., 2016; Shinde, 2016; Shinde and Shukla, 2017). The IR spectra of Mg_n (n = 2–31) nanoclusters were studied using DFT, and the results showed that their most intense peaks were distributed in the low-frequency band of 40–270 cm^{-1} (Belyaev et al., 2016). The linear absorption spectroscopy studies of very small size Mg_n (n = 2–5) nanoclusters confirm that their low-lying structures, although small, can be experimentally distinguished, while the optical excitation spectra are confirmed to be of plasmonic collective type (Shinde, 2016).

In short, nanocluster materials, like Au and Mg, are a field of materials science full of unknown "surprises" where many interesting optical and electronic excitation properties can be "discovered". However, surprisingly, the study of gold-doped Mg nanoclusters has not been reported so far. This work aims to perform a systematic theoretical computational study of the structural and optical properties of gold-doped small-size magnesium nanoclusters. Specifically, the geometric growth mechanism, relative stability, charge transfer properties, chemical bonding properties, nonlinear optical properties, and theoretical calculations of infrared and Raman-weighted average spectra of $AuMg_n$ (n = 2–12) nanoclusters will be investigated. These studies will not only enrich the research data on $AuMg_n$ nanoclusters, but also provide the opportunity to gain insight into potential nanomaterials with interesting optical properties.

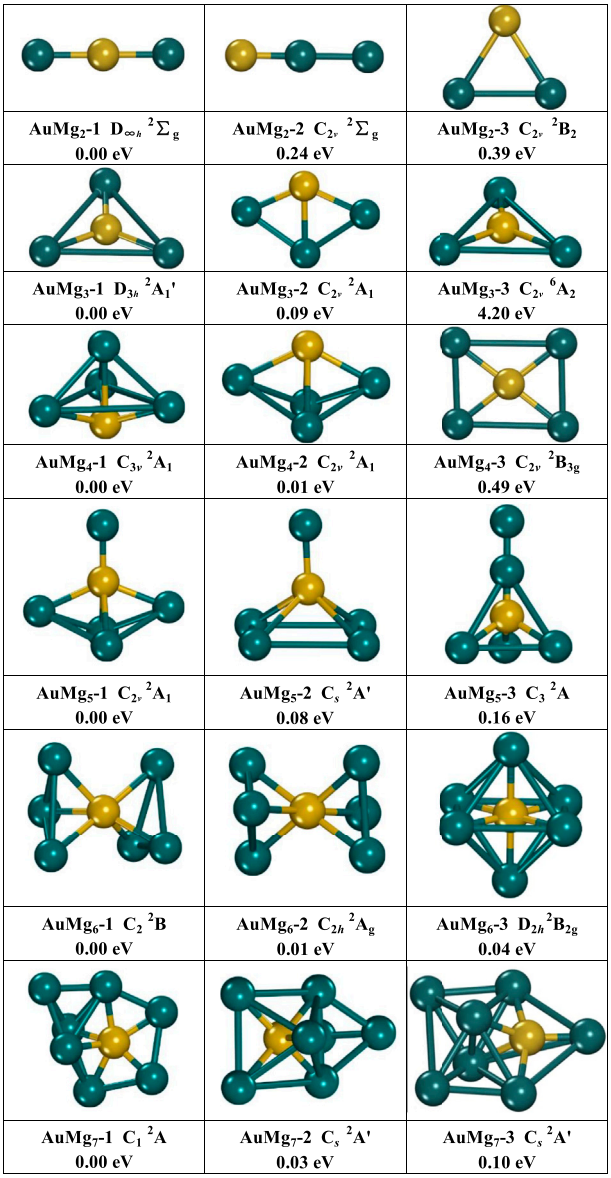

FIGURE 1 | The geometry of the three lowest energy isomers of $AuMg_n$ (n = 2–7) nanoclusters, energy difference in eV from the lowest energy isomer at the same size.

COMPUTATIONAL METHOD DETAILS

CALYPSO software (Wang et al., 2010, 2012) was utilized to search the initial geometries of $AuMg_n$ (n = 2–12) nanoclusters. CALYPSO can perform predictions of the energetically low-lying isomers structures at given chemical compositions and pressure for nanoclusters (Lv et al., 2012; Zhao et al., 2019; Lu et al., 2020) in gas-phase and crystals (Lu and Chen, 2020a, 2020b, 2021; Sun et al., 2020; Chen et al., 2021) *via* particle swarm optimization (PSO) algorithm. To search for as many low-lying energy isomers of $AuMg_n$ (n = 2–12) nanoclusters as possible, the following strategy will be employed. First, each size of AuMgn nanocluster will be searched for 50 generations, where each generation contains 20 structures. Further, 80% of these 1,000 heterogeneous structures are generated by the PSO algorithm for the initial structure, and the rest are generated randomly. These structures are then interfaced *via* CALYPSO to Gaussian 09 software (Frisch et al., 2016) for low-level HF energy calculations, and finally ranked by energy level. It is necessary to explain that many of the 1,000 isomers obtained have the same or extremely close energies, and their geometrical structures do

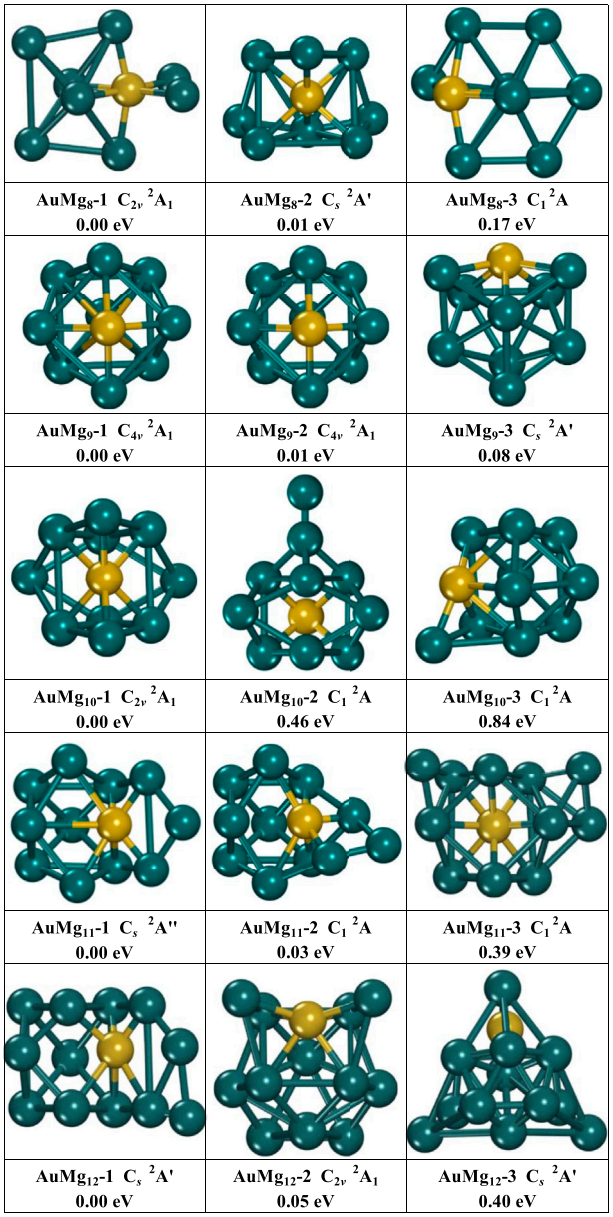

FIGURE 2 | The geometry of the three lowest energy isomers of $AuMg_n$ (*n* = 8–12) nanoclusters, energy difference in eV from the lowest energy isomer at the same size.

not differ much and therefore need to be removed. Finally, isomers with significantly different energies and structures were again subjected to high-level DFT for structural optimization and frequency calculations by Gaussian 09 software. The structure optimization calculation employs the classical B3LYP functional, where the mixed basis set is considered due to the presence of Au atom. Concretely, 6–311 g (d) is applied to Mg atoms, while the pseudopotential basis set lanl2dz is used for Au atoms. The adoption of such functional and basis set is based on the following two aspects, firstly, the existing studies have shown that Mg_n nanoclusters do not have any metallic properties at the size of $n < 20$ (Köhn et al., 2001; Jellinek and Acioli, 2003; Xia et al., 2016), and secondly, all-electron basis set and lanl2dz basis set have been proved to be reliable for Mg and Au nanoclusters by numerous studies (Xia et al., 2016; Zeng et al., 2020; Zhu et al., 2021). To ensure a more comprehensive structural optimization, each isomer was calculated under 2, 4, 6, and 8 spin multiplicities, respectively. In addition, to verify that the isomer is not a transition or excited state, imaginary frequencies must be excluded from any result. Once the imaginary frequency appears in the calculation result, they need to be optimized again until all frequencies are positive.

Charge transfer property of the lowest energy $AuMg_n$ (*n* = 2–12) nanoclusters was analyzed by natural bond orbital (NBO) calculation (Reed et al., 1988). Chemical bonding properties were computed through the electron localization function (ELF) (Becke and Edgecombe, 1990). The nonlinear optical properties of the ground state $AuMg_n$ nanoclusters were investigated at the aug-cc-pVTZ level. Infrared and Raman spectra are the results of vibration frequency calculations. In particular, Multiwfn software (Lu and Chen, 2012) is a powerful tool to draw 2D map of ELF, spherical plots of static and super-static polarizabilities, Boltzmann distribution probabilities of different isomers and weighted average IR and Raman spectral data.

RESULTS

The Geometrical Growth Mechanism of $AuMg_n$ Nanoclusters

The growth mechanism of nanoclusters can be studied by their geometric structures. Three low-lying energy isomers of each size $AuMg_n$ (*n* = 2–12) nanoclusters are presented in **Figure 1** and **Figure 2**. Under each structure, the "i" in $AuMg_n$-i is their energy order, with "1" indicating the lowest and "2" the second-lowest ones. The energy difference (eV) between the AuMgn-i and $AuMg_n$-1 at each size can also be found. In addition to the symmetry, and the electronic structure information is also shown in **Figures 1**, **2**. All information about the lowest energy state of $AuMg_n$ (*n* = 2–12) nanoclusters is summarized in **Table 1**, where the results of the frequency calculations show the lowest and highest vibrational frequencies satisfying the requirements that the results of the frequency calculations cannot contain any imaginary frequency. As can be seen from **Figure 1**, isomers $AuMg_2$-1 ($D_{\infty h}$ symmetry with $^2\Sigma_g$ electronic state) and $AuMg_2$-2 (C_{2v} symmetry with $^2\Sigma_g$ electronic state) have a similar linear structure, the difference being that the Au atom is in the center of the former and on the side of the latter. Isomers $AuMg_2$-3 (C_{2v} symmetry with $^2B_2$ electronic state) show a 2D planar isosceles triangle structure. Relative to the lowest energy state $AuMg_2$-1 isomer energy, $AuMg_2$-2 and $AuMg_2$-3 isomers have 0.24 and 0.39 eV higher energy than it, respectively. The isomer $AuMg_3$-1 (D_{3h} symmetry with $^2A'_1$ electronic state) has an equilateral triangular geometry, while the isomer $AuMg_3$-3 (C_{2v} symmetry with $^6A_2$ electronic state) has an isosceles triangular structure, and interestingly the Au atoms are located at the center of their triangular structures, respectively. The structure of the isomer

TABLE 1 | State, symmetry, Eb, Δ_2E, Egap for α- and β-electrons, frequency and NCP on Au atom in the ground state of $AuMg_n$ (*n* = 2–12) nanoclusters.

Clusters	State	Symmetry	E_b(eV)	Δ_2E(eV)	$E_{gap}\alpha$(eV)	$E_{gap}\beta$(eV)	Frequency (cm^{-1})		NCP on Au (e)
							Highest	Lowest	
$AuMg_2$	$D_{\infty h}$	$^2\sum_g$	1.72	—	2.76	2.53	220	14	–0.74
$AuMg_3$	D_{3h}	$^2A_1'$	1.78	–0.15	2.28	2.22	197	25	–1.35
$AuMg_4$	C_{3v}	$^2A_1$	1.84	0.29	2.19	2.15	212	23	–1.68
$AuMg_5$	C_{2v}	$^2A_1$	1.83	–0.03	2.28	1.29	232	13	–2.17
$AuMg_6$	C_2	^2B	1.83	–0.04	2.21	1.14	225	9	–2.99
$AuMg_7$	C_1	^2A	1.84	–0.05	1.74	1.65	207	10	–2.44
$AuMg_8$	C_{2v}	$^2A_1$	1.85	–0.32	1.55	1.58	203	20	–3.05
$AuMg_9$	C_{4v}	$^2A_1$	1.89	0.24	1.63	1.75	236	53	–1.00
$AuMg_{10}$	C_{2v}	$^2A_1$	1.90	0.28	1.14	1.85	224	21	–2.49
$AuMg_{11}$	C_s	$^2A''$	1.89	–0.12	1.70	1.39	232	27	–2.39
$AuMg_{12}$	C_s	$^2A'$	1.88	—	1.15	1.88	243	13	–2.47

$AuMg_3$-2 (C_{2v} symmetry with $^2A_1$ electronic state) is a planar combination of Au-Mg-Mg isosceles triangle and Mg-Mg-Mg isosceles triangle. Calculations show nanoclusters of 2 Mg atoms doped with one Au atom, where the second and third lowest isomers are 0.03 and 4.20 eV higher than the lowest energy isomer, respectively. The structures of the isomers $AuMg_4$-1 (C_{3v} symmetry with $^2A_1$ electronic state) and $AuMg_4$-2 (C_{2v} symmetry with $^2A_1$ electronic state) can be considered as formed based on the tetrahedral (pyramid-like) structure of Au-Mg-Mg-Mg adsorbing an Mg atom in different directions. The isomer $AuMg_4$-3 (C_{2v} symmetry with $^2B_{3g}$ electronic state) shows a rectangular structure in which the 4 Mg atoms are at the vertices while Au atom is at the geometric center. For the isomer $AuMg_4$-1, $AuMg_4$-2 and $AuMg_4$-3 are higher in energy by 0.01 and 0.49 eV, respectively. The structure of the isomer $AuMg_5$-1 (C_{2v} symmetry with $^2A_1$ electronic state) is based on the formation of $AuMg_4$-2 by adsorbing an Mg atom on its top. The isomers $AuMg_4$-3 and $AuMg_4$-1 form the isomers $AuMg_5$-2 (C_s symmetry with $^2A'$ electronic state) and $AuMg_5$-3 (C_3 symmetry with ^2A electronic state) after pulling up the Au atom into the interior of the polyhedral while adsorbing an Mg atom on their tops. The second- and third-lowest energy isomers of the $AuMg_5$ nanocluster are 0.08 and 0.16 eV higher than that of the lowest-energy isomer. The isomers $AuMg_6$-1 (C_2 symmetry with ^2B electronic state) and $AuMg_6$-2 (C_{2h} symmetry with ^2A_g electronic state) have extremely close energies and structures, which exhibit rotational symmetry with Au atom. The isomer $AuMg_6$-3 ($^2B_{2g}$ electronic state), which is higher 0.04 eV in energy than $AuMg_6$-1, possesses a high symmetry (D_{2h}) octahedron in which the Au atom is located at its center. The structures of the isomers $AuMg_7$-1 (C_1 symmetry with ^2A electronic state), $AuMg_7$-2 (C_s symmetry with $^2A'$ electronic state) and $AuMg_7$-3 (C_s symmetry with $^2A'$ electronic state) are all grown based on the diversity of Au-Mg-Mg-Mg tetrahedra-like geometries. In addition, the energy shift of the isomers $AuMg_7$-2 and $AuMg_7$-3 relative to the lowest energy state are 0.03 and 0.10 eV, respectively.

As **Figure 2** displayed, the medium-sized $AuMg_n$ (8–12) nanoclusters exhibit a diversity of structures. The structures of the isomers $AuMg_8$-1 (C_{2v} symmetry with $^2A_1$ electronic state) and $AuMg_8$-3 (C_1 symmetry with ^2A electronic state) are generated based on the deformation of $AuMg_7$-3 after adsorption of an Mg atom, while the structure of the isomer $AuMg_8$-2 (C_s symmetry with $^2A'$ electronic state) can be obtained from the deformation of $AuMg_7$-2 by adsorption of an Mg atom. The second and third lowest energy isomers of $AuMg_8$ nanoclusters are higher in energy than the ground state by 0.01 and 0.17 eV. The isomers $AuMg_9$-1 and $AuMg_9$-2 have the same symmetry (C_{4v}), electronic structure ($^2A_1$), energy and "fascinating cage-like" structures. The isomer $AuMg_9$-3 ($^2A'$ electronic state), which is 0.08 eV higher in energy than $AuMg_9$-1, has a cage-like structure with C_s symmetry. The structures of the isomers $AuMg_{10}$-1 (C_{2v} symmetry with $^2A_1$ electronic state), $AuMg_{10}$-2 (C_1 symmetry with ^2A electronic state) and $AuMg_{10}$-3 (C_1 symmetry with ^2A electronic state) are generated based on the deformation of $AuMg_9$-1 by adsorption of Mg atoms in different directions. The second and third lowest energy isomers of $AuMg_{10}$ nanoclusters are higher in energy than the first lowest energy by 0.46 and 0.84 eV, respectively. Interestingly, the isomers $AuMg_{11}$-1 (C_s symmetry with $^2A'$ electronic state) and $AuMg_{11}$-2 (C_1 symmetry with ^2A electronic state) are easily obtained by the deformation of $AuMg_{10}$-2 by adsorption of an Mg atom. On the other hand, $AuMg_{11}$-3 (C_1 symmetry with ^2A electronic state) is formed by the deformation of AuMg10-1 after the adsorption of an Mg atom. $AuMg_{11}$-2 and $AuMg_{11}$-3 have higher energies than $AuMg_{11}$-1 at 0.03 and 0.39 eV. The isomer $AuMg_{12}$-1 (C_s symmetry with $^2A'$ electronic state) is generated by the adsorption of an Mg atom by $AuMg_{11}$-1. The isomer $AuMg_{12}$-2 (C_{2v} symmetry with $^2A_1$ electronic state), on the other hand, exhibits a deformed tubular-like structure, while the isomer $AuMg_{12}$-3 (C_s symmetry with $^2A'$ electronic state) has a pyramid-like structure. Furthermore, compared to the energy of $AuMg_{12}$-1, $AuMg_{12}$-2 and $AuMg_{12}$-3 are 0.05 and 0.40 eV higher, respectively. Because the lowest energy state isomers of nanoclusters often require more comprehensive studies to explore their various physical and chemical properties, the atomic coordinates of the $AuMg_n$-1 (*n* = 2–20) nanoclusters are shown in **Supplementary Table S1** in the Supplemental Material.

In conclusion, based on the small size of $AuMg_{n-1}$ or smaller, $AuMg_n$ (*n* = 2–12) nanoclusters can usually be formed by

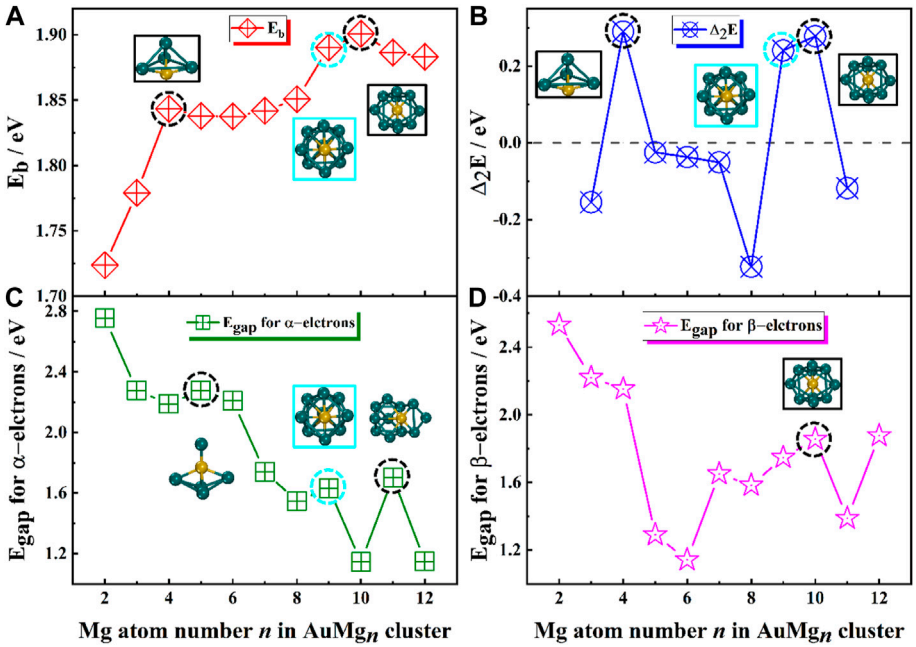

FIGURE 3 | (A) Average binding energy E_b, **(B)** The second order difference energy Δ_2E, **(C)** The HOMO-LUMO energy gap E_{gap} for α-electrons, **(D)** The HOMO-LUMO energy gap E_{gap} for β-electrons in the ground state of $AuMg_n$ (*n* = 2–12) nanoclusters.

adsorption of Mg atoms in different directions, and the interesting point is that the direction of adsorption does not have a fixed pattern. Such result is consistent with many existed Mg-based nanoclusters reported (Li et al., 2017; Zeng et al., 2020, 2021; Zhu et al., 2020). However, despite the many similarities, the structures of gold-doped Mg nanoclusters have unique properties compared to other Mg-based nanoclusters studies. For example, the structure of $AuMg_3$ nanoclusters is 2D planar, while the lowest energy heterostructures of Be (Zeng et al., 2020), Si (Zhu et al., 2020), C, Ge, Sn (Zeng et al., 2021), Zn-doped (Li et al., 2017) Mg nanoclusters of corresponding sizes are all ortho-tetrahedral in shape. Interestingly, although the ground-state structures of $AuMg_9$ and $BeMg_9$ (Zeng et al., 2020) look similar, the significant difference between them is that the Au atom locates on the surface of $AuMg_9$ while the Be atom is absorbed into the inside of $BeMg_9$.

The Relative Stabilities

Since clusters exhibit different physical and chemical properties at different sizes, their relative stability is well worth studying. The relative stability of cluster can be calculated through the following three quantities, that is the binding energy per atom (E_b in eV), the second-order energy difference (Δ_2E in eV) and the HOMO-LUMO energy gap (E_{gap} in eV). **Equations 1–3** display the above three energies for $AuMg_n$-1 (*n* = 2–20) nanoclusters in **Figure 1**.

$$E_b(AuMg_n) = [nE(Mg) + E(Au) - E(AuMg_n)]/(n+1) \quad (1)$$

$$\Delta_2E(AuMg_n) = E(AuMg_{n+1}) + E(AuMg_{n-1}) - 2E(AuMg_n) \quad (2)$$

$$E_{gap}(AuMg_n) = E_{LUMO}(AuMg_n) - E_{HOMO}(AuMg_n) \quad (3)$$

E (Au) and *E* (Mg) denote the energies of free Au and Mg atoms, *E* ($AuMg_n$) means the energy of the corresponding nanocluster. The lowest unoccupied molecular orbital (LUMO) and highest occupied molecular orbital (HOMO) energies are E_{LUMO} and E_{HOMO}.

The theoretically calculated values of these quantities for $AuMg_n$-1 (*n* = 2–20) nanoclusters are presented in **Table 1** and their curves with size are showed in **Figure 3**. As **Figure 3A** displayed, overall, the E_b curve becomes larger as the size of the nanoclusters increases, implying that the atoms within the $AuMg_n$ nanoclusters bind more stably as the Au atoms are doped. Locally, the maximum value of E_b appears at $AuMg_{10}$ (1.90 eV), indicating that this nanocluster has the robust stability. Secondly, a small local peak (1.84 eV) appears at $AuMg_4$, indicating that it is slightly more stable than its neighbors. **Figure 3B** shows the curve of the Δ_2E, which can be detected experimentally by mass spectrometry. Interestingly, as in the case of the local peaks of the E_b curve, $AuMg_4$ and $AuMg_{10}$ have local maximum Δ_2E values of 0.29 and 0.28 eV, respectively. This conclusion suggests that they are both the most stable and have a high probability of being observed in mass spectrometry experiments. The thermodynamic stability of nanoclusters can be characterized by the value of their E_{gap}. Since $AuMg_n$ nanoclusters are open-shell systems, they have both α and β-electrons, and the E_{gap} of α and β-electrons are illustrated in **Figure 3C** and **Figure 3D**. For α-electrons E_{gap} curve of $AuMg_n$ nanoclusters, the local peaks appear at *n* = 5, 9 and 11, while $AuMg_{10}$ has the largest local β-electron E_{gap}, indicating that the thermal stability of these clusters is relatively high.

In conclusion, $AuMg_4$ and $AuMg_{10}$ nanoclusters show the robust stability. However, it is noteworthy that the $AuMg_9$

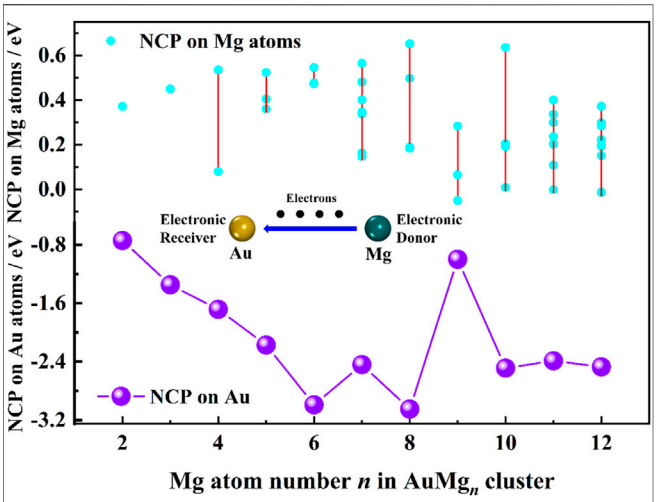

FIGURE 4 | NCP analysis on Au and Mg atoms in the ground state of $AuMg_n$ (*n* = 2–12) nanoclusters.

nanocluster is always the second largest value in both E_b and Δ_2E curves, although they are not the maximum values. Therefore, combined with the E_{gap} maximum for α-electrons, $AuMg_9$ nanocluster also has considerable robust stability and be worthy studying.

Charge Transfer Property and Chemical Bond Analysis

The natural charge population (NCP) results from the NBO calculations can reveal the charge transfer properties in the nanoclusters. The NCP values of Au atoms in **Table 1** are in the range of [−2.99, −0.74] e, indicating that Au atoms play the role of electron receiver in all nanoclusters. The curve of NCP on Au atom with the size is ploted in **Figure 4**. The $AuMg_9$ nanocluster appears to be very special, which is probably originated from its high symmetry structure. **Supplementary Table S2** in the Supplementary Material shows the NCP values on the Mg atoms. Except for 4 Mg atoms in $AuMg_9$ with a charge of −0.05 e and 1 Mg atom in $AuMg_{12}$ with an NCP value of −0.01 e, all other Mg atoms have positive NCP values, distributed from 0.65 to 0.01 e, suggesting that they are losing electrons. In other words, Mg atoms are electron donors in the $AnMg_n$ nanoclusters. The charge transfer property depends on the electronegativity of the atom, the greater the electronegativity, the easier it is to get electrons. The electronegativity value of Mg atom is 1.31, while that of Au atom is 2.54, so the charge transfer is mostly from Mg atom to Au atom.

The ELF values of atomic bonding regions and their 2D maps are useful tools for analyzing the chemical bonding properties of nanoclusters. ELF is a value greater than 0 and less than 1, which characterizes the degree of electron localization and thus can determine the bonding properties. A region with ELF > 0.5 implies high electron localization and covalent bonding in the bonding region, while a region with ELF < 0.5 has low electron localization and non-covalent bonding in the bonding region. **Figure 5** and **Supplementary Figure S1** in the Supplementary Material display the 2D distribution of the EFL value for the ground state $AuMg_n$ (*n* = 2–12) nanoclusters. The calculations show that Mg-Mg in $AuMg_n$ nanoclusters is covalently bonded, while Au-Mg bond is non-covalent. The relatively large value of ELF around Au atom and low in bonding region indicates that the valence layer of Au atom is solidified around it, so it does not form covalent bonds with Mg. Furthermore, considering that the Au atom always gains electrons and the Mg atom around it loses electrons to be positively charged, it can be concluded that Au-Mg is ionic bonding. Another noteworthy point is that the critical size for Mg-Mg bonding is $AuMg_4$. ELF distribution map shows that Mg-Mg does not covalently bond in $AuMg_2$ and $AuMg_3$ nanoclusters.

The Nonlinear Optical Property

Static polarizabilities α (∞) and hyperpolarizabilities β (∞) for the ground state $AuMg_n$ (*n* = 2–20) nanoclusters were calculated to analyze their nonlinear optical property. Specifically, the coupled-perturbed Kohn-Sham (CPKS) method (Jensen, 2017) was adopted for the $AuMg_n$ nanoclusters to compute the polarizabilities and hyperpolarizabilities in the zero-frequency limit (λ→∞). The results of α(∞) and β(∞) calculations are presented in **Supplementary Table S3** in the Supplementary Material and are shown in **Figure 6**. From **Figure 6A**, it can be seen that the polarization anisotropy α_{aniso} (∞) and isotropy α_{iso} (∞) of $AuMg_n$ nanoclusters do not change consistently with the size. The α_{iso} (∞) shows an overall upward trend, except for $AuMg_9$, while the α_{aniso} (∞) oscillates with increasing size. In addition, α_{xx} (∞), α_{yy} (∞), α_{zz} (∞) of each nanocluster are also shown in **Figure 6A**. Due to the diversity of the nanoclusters structures, these quantities display irregular oscillations in different directions. However, $AuMg_9$ nanocluster with high structural symmetry exhibits synchronous local minimum anisotropic and isotropic polarization, suggesting that it has special nonlinear optical properties compared to other nanoclusters. In order to study the polarization of $AuMg_9$ more intuitively, the unit sphere representation of its polarization tensor is plotted in **Figure 6C**. One can find the anisotropic polarization of $AuMg_9$, more specifically, the small polarization rate in the x-y plane and the maximum polarization rate in the z-direction (i.e., the direction of the line connecting the leftmost Au and the rightmost Mg in the figure).

Figure 6B exhibits the static hyperpolarizability β (∞) of the $AuMg_n$ nanoclusters and their projection values in the dipole moment direction β_{prj} (∞). Since β_{prj} (∞) can be measured by the electric field-induced second harmonic generation experiment (EFISH), it serves as a guide for experiments. Specifically, β increases from $AuMg_2$ to a maximum value of $AuMg_5$, then gradually decreases to a minimum value of $AuMg_9$, and increases again afterward. Interestingly, the β and β_{prj} of $AuMg_9$ and the nanoclusters smaller than it are exactly equal, indicating that its β is isotropic with the dipole moment. However, starting from $AuMg_{10}$ nanocluster, the two curves are reversed, forming a mirror-symmetric trend. **Figure 6D** shows the unit sphere representation of static

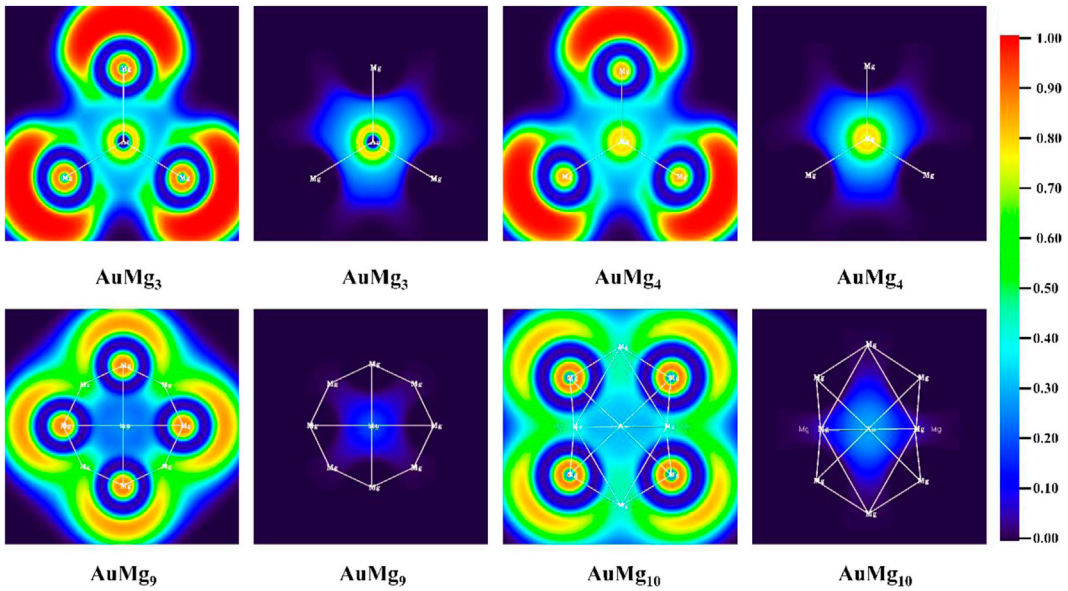

FIGURE 5 | The ELF analysis for Mg-Mg and Au-Mg chemical bonds for $AuMg_n$ (*n* = 3, 4, 9, 10) nanoclusters.

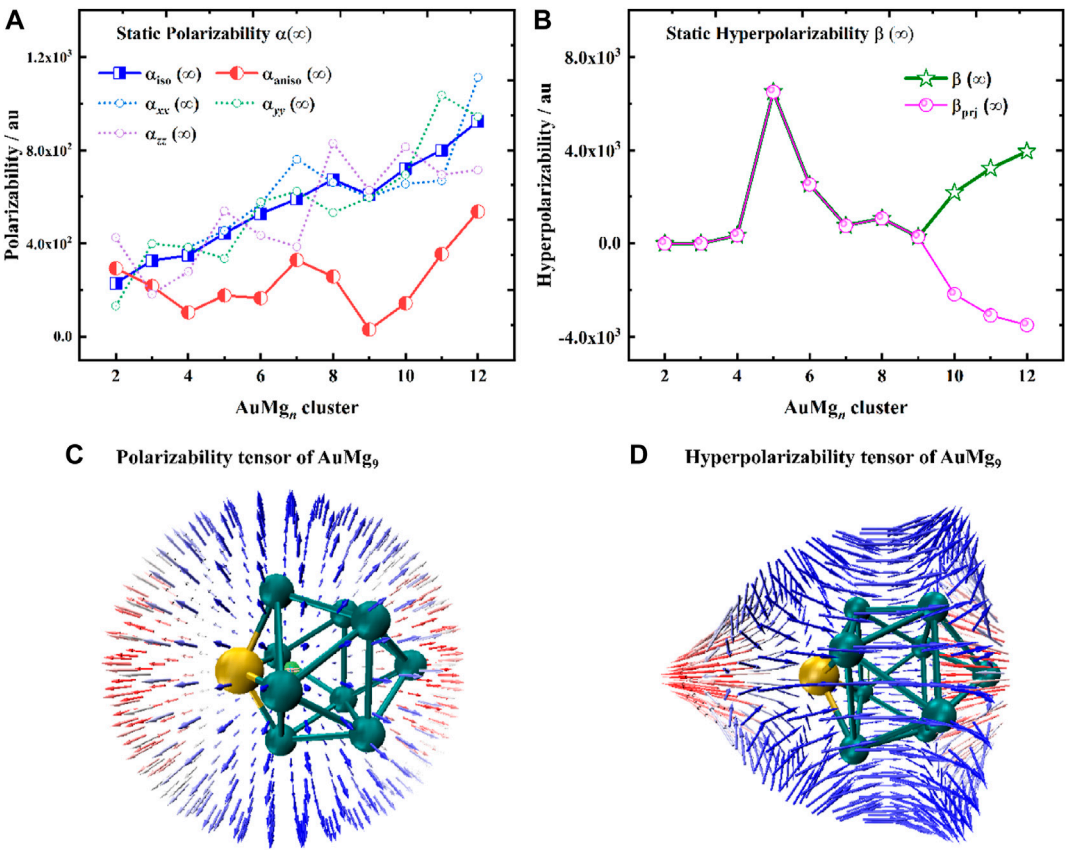

FIGURE 6 | (A) Static polarizabilities α(∞), **(B)** Static hyperpolarizabilities β(∞) for the ground state of $AuMg_n$ (*n* = 2–12) nanoclusters, **(C)** The unit sphere representation of static polarizability tensor α, **(D)** The unit sphere representation of static hyperpolarizability tensor β of $AuMg_9$ nanocluster.

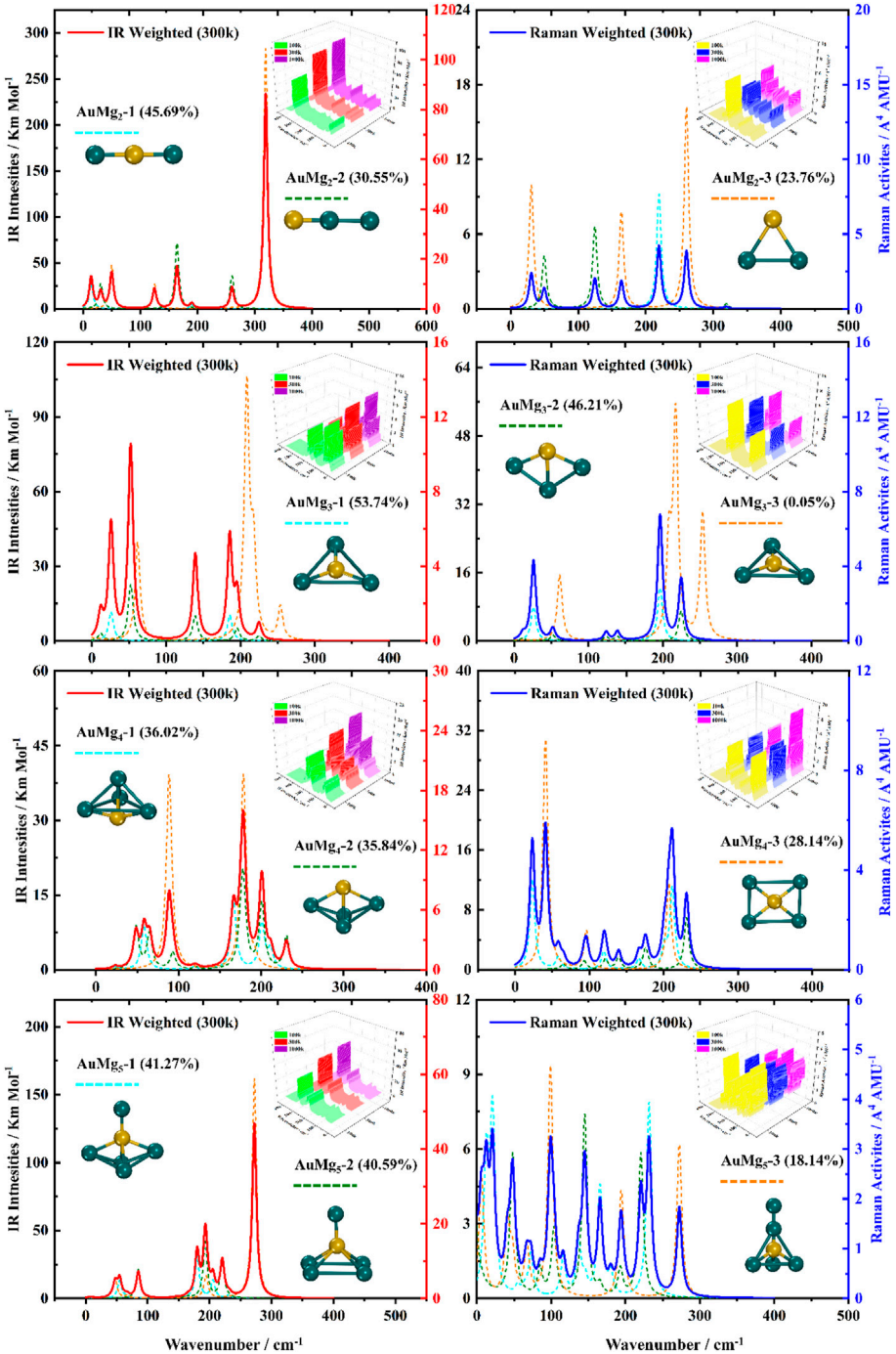

FIGURE 7 | Boltzmann distribution weighted average spectra of the three lowest energy isomers of $AuMg_n$ (*n* = 2–5) nanoclusters at room temperature (IR on the left side, Raman on the right side).

hyperpolarizability tensor β of $AuMg_9$, it is found that β is also anisotropic, with a maximum in the z-direction, and changes in the x-y plane as the Mg atoms surround it. In conclusion, relative to other nanoclusters, AuMg9 exhibits distinctive nonlinear optical properties.

Boltzmann Distribution Weighted Average Spectra of IR and Raman

For the ground state $AuMg_n$ nanoclusters, the infrared and Raman spectra with weighted average of the Boltzmann distribution were calculated for guidance experiments. The

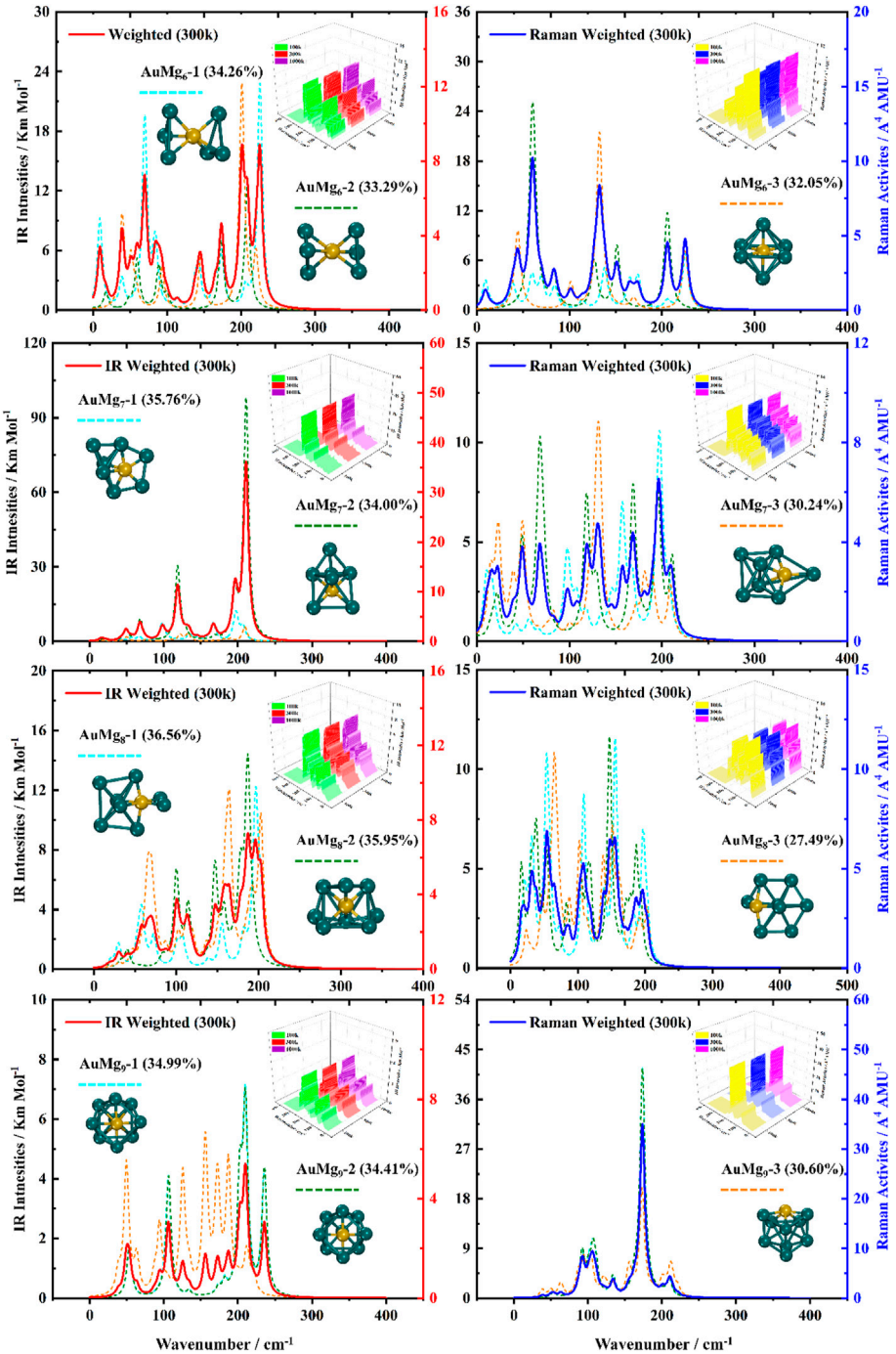

FIGURE 8 | Boltzmann distribution weighted average spectra of the three lowest energy isomers of $AuMg_n$ (*n* = 6–9) nanoclusters at room temperature (IR on the left side, Raman on the right side).

motivation for considering the Boltzmann distribution is due to the difficulty of observing only the ground state nanoclusters in experiments, especially in the gas-phase nanoclusters. **Figure 7** display the IR and Raman spectra of the weighted average of the Boltzmann distribution at room temperature. The Boltzmann distribution probabilities of each isomer at different temperatures were also calculated by the relevant equations in the Supplementary Material. The small 3D plots in each map are the corresponding weighted average spectra at 100 k, 300 k and 1000 k temperatures. As shown in **Figures 7–9**, the strongest absorption peaks of IR spectra are distributed in the 40–350 cm^{-1} frequency band, while the strongest peaks of Raman spectra are

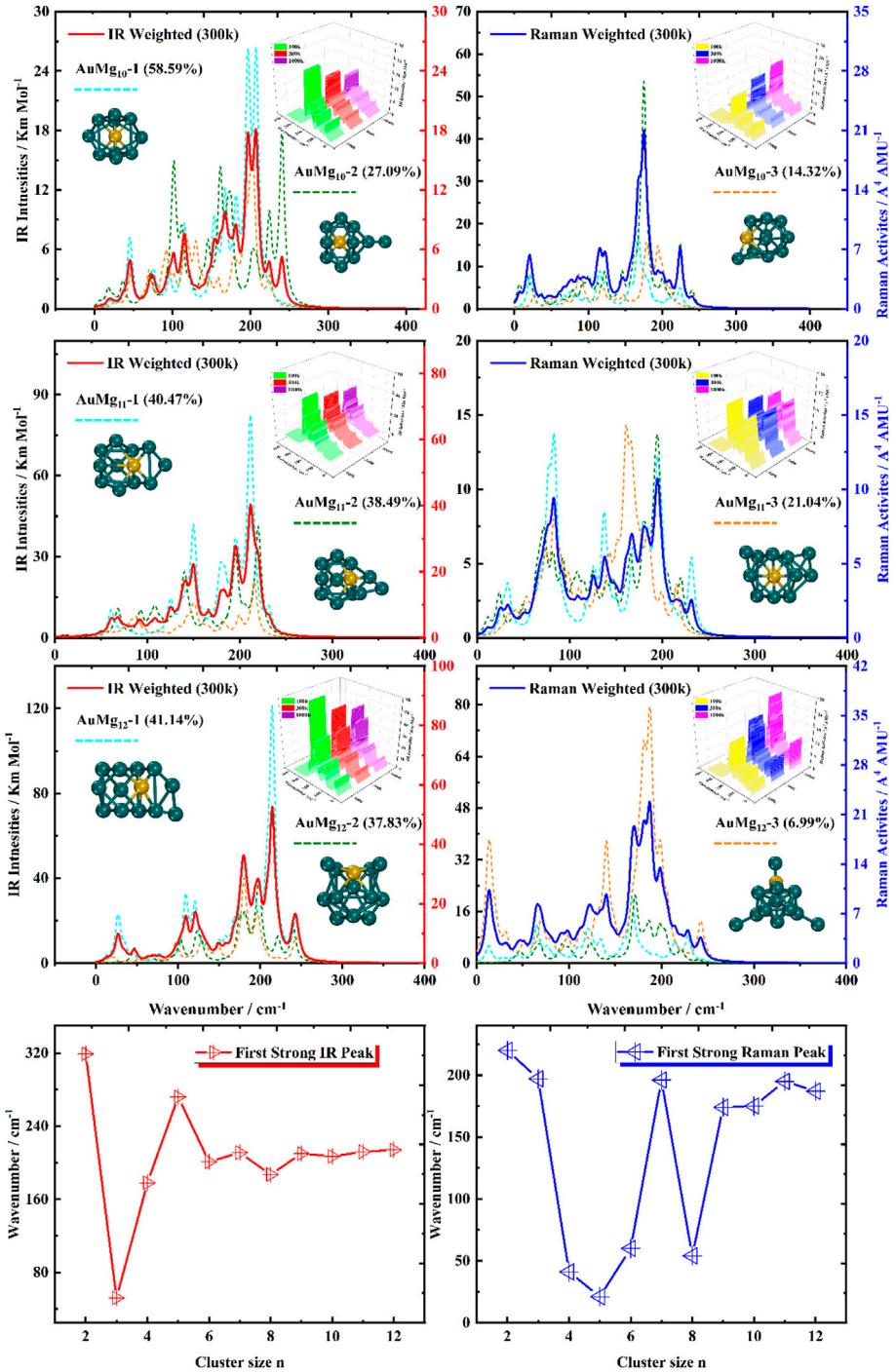

FIGURE 9 | Boltzmann distribution weighted average spectra of the three lowest energy isomers of $AuMg_n$ (*n* = 10–12) nanoclusters at room temperature (IR on the left side, Raman on the right side), and the first strong IR and Raman peaks in $AuMg_n$ (*n* = 2–12) nanoclusters.

distributed in a narrower band of 20–220 cm^{-1}. However, the most intense peaks of both IR and Raman weighted average spectra appear around 200 cm^{-1} as the size increases. In addition, as can be seen from the small 3D plots in each figure and **Supplementary Figure S2** in the Supplementary Material, the location of the most intense peak of the weighted average spectrum does not shift as the temperature increases, but the intensity changes.

Specifically, for the weighted average IR spectra at room temperature, the nanoclusters of $AuMg_n$ (*n* = 4–12) are easily distinguished as separate strong bands in the 200 cm^{-1} regions of the spectra, except for the $AuMg_2$ and $AuMg_3$ nanoclusters. This

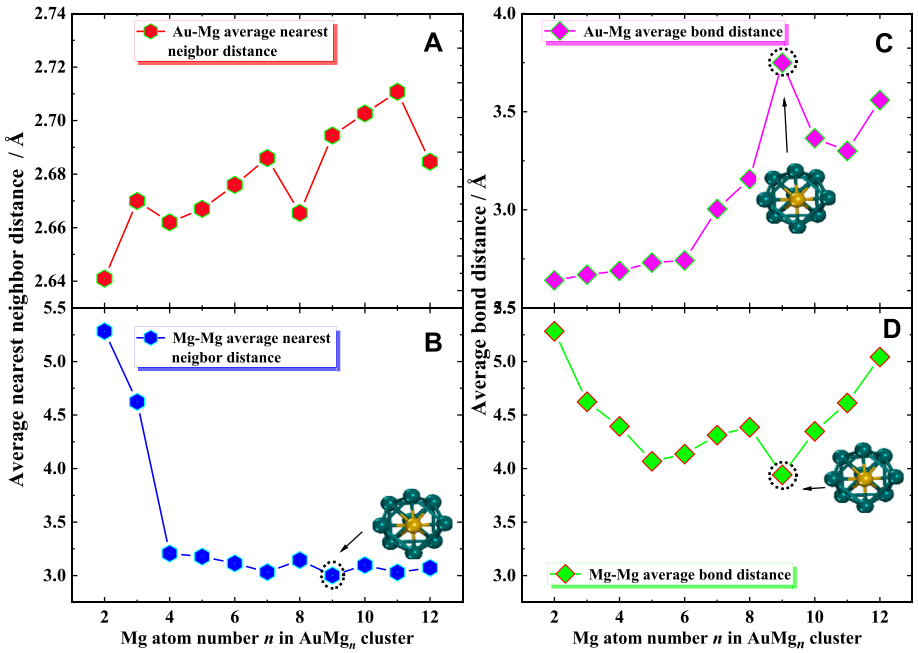

FIGURE 10 | (A,B) Average nearest neighbor distance for Au-Mg and Mg-Mg, **(C,D)** Average bond distance for Au-Mg and Mg-Mg.

result is in good agreement with the results of infrared spectroscopy of pure Mg nanoclusters studied by Belyaev et al. (Belyaev et al., 2016). For the Raman weighted average spectrum at room temperature, although the strongest Raman activity peaks of $AuMg_4$, $AuMg_5$ and $AuMg_6$ nanoclusters appear in the low-frequency band (20–50 cm^{-1}), they still have many strong peaks in the 200 cm^{-1} regions. Therefore, for all the Raman spectra of the $AuMg_n$ (n = 2–12) nanoclusters, the 200 cm^{-1} regions can be more easily distinguished as individual strong bands. In conclusion, it was computationally shown that the formation of $AuMg_n$ (n = 2–12) nanoclusters at room temperature is possible to identify these nanoclusters by IR and Raman spectroscopy.

The Average Bond Distance and Average Nearest Neighbor Distance

In order to provide more data support for future possible experiments, the average bond distance and average nearest neighbor distance were calculated. As shown in **Figure 10**, the average nearest neighbor distance and bond distance for Au-Mg and Mg-Mg in the ground state of $AuMg_n$ (n = 2–12) clusters display some interesting conclusions. **Figures 10A,B** show that, overall, the nearest neighbor distance for Au-Mg becomes larger as the cluster size increases (except for n = 8 and 12), while Mg-Mg is overall decreasing. The average nearest neighbor distance of Au-Mg is 2.68 Å, and that of Mg-Mg is 3.44 Å. **Figure 10C** gives the average bond distance of Au-Mg with cluster size dependence similar to the nearest neighbor distance of Au-Mg, i.e., increasing overall. However, **Figure 10D** demonstrates that the average Mg-Mg bond distance decreases and then increases with cluster size. Another interesting conclusion is that the local turning points of the average bond and nearest-neighbor distances for Mg-Mg and the average bond distance curves for Au-Mg occur at $AuMg_9$, suggesting that they influence the local stability of the clusters.

CONCLUSION

In this work, the structure of Au-doped Mg_n (n = 2–12) nanoclusters was investigated by CALYPSO crystal search software. It is shown that the geometric growth mechanism of this nanocluster has similarities to other atom-doped Mg_n clusters but also has unique features, such as the planar structure of $AuMg_3$ and the high symmetry cage-like structure of $AuMg_9$. Stability calculations show that $AuMg_4$ and $AuMg_{10}$ have high local stability, while $AuMg_9$ nanoclusters are the second most stable nanoclusters. The charge transfer study reveals that Au atoms are electron receivers and Mg atoms are electron donors in $AuMg_n$ nanoclusters. ELF analysis showed that Mg-Mg formed a covalent chemical bond while Au-Mg was an ionic bond, and the critical size for the appearance of the Mg-Mg covalent bond was found to be $AuMg_3$. The nonlinear optical properties of $AuMg_n$ nanoclusters were probed by calculating the static polarizability and hyperpolarizability, and the results indicate that $AuMg_9$ is a special one of interest. Boltzmann distribution weighted average IR and Raman spectroscopy studies at room temperature confirm that these nanoclusters can be identified by spectroscopic experiments. Finally, the average bond distance and average nearest neighbor distance were fully investigated.

DATA AVAILABILITY STATEMENT

The original contributions presented in the study are included in the article/**Supplementary Material**, further inquiries can be directed to the corresponding authors.

AUTHOR CONTRIBUTIONS

B-CZ: Software, Investigation, Writing Original draft preparation. P-JD: Methodology, Investigation, Data curation, Visualization. JG: Data curation, Visualization. W-BK: Conceptualization, Methodology, Formal analysis, Investigation, Writing review and editing.

FUNDING

This work is supported partly by National Natural Science Foundation of China (No. 11947006), and partly by the Cultivating Project for Young Scholar at Hubei University of Medicine (No. 2019QDJZR12).

SUPPLEMENTARY MATERIAL

The Supplementary Material for this article can be found online at: https://www.frontiersin.org/articles/10.3389/fchem.2022.870985/full#supplementary-material

REFERENCES

Alvarez, M. M., Khoury, J. T., Schaaff, T. G., Shafigullin, M., Vezmar, I., and Whetten, R. L. (1997). Critical Sizes in the Growth of Au Clusters. *Chem. Phys. Lett.* 266, 91–98. doi:10.1016/S0009-2614(96)01535-7

Assadollahzadeh, B., and Schwerdtfeger, P. (2009). A Systematic Search for Minimum Structures of Small Gold Clusters Au[sub N] (N=2-20) and Their Electronic Properties. *J. Chem. Phys.* 131, 064306. doi:10.1063/1.3204488

Becke, A. D., and Edgecombe, K. E. (1990). A Simple Measure of Electron Localization in Atomic and Molecular Systems. *J. Chem. Phys.* 92, 5397–5403. doi:10.1063/1.458517

Belyaev, S. N., Panteleev, S. V., Ignatov, S. K., and Razuvaev, A. G. (2016). Structural, Electronic, Thermodynamic and Spectral Properties of Mgn (N=2-31) Clusters. A DFT Study. *Comput. Theor. Chem.* 1079, 34–46. doi:10.1016/j.comptc.2016.01.011

Chen, B., Conway, L. J., Sun, W., Kuang, X., Lu, C., and Hermann, A. (2021). Phase Stability and Superconductivity of lead Hydrides at High Pressure. *Phys. Rev. B* 103, 035131. doi:10.1103/PhysRevB.103.035131

Chen, H., Liang, H., Dai, W., Lu, C., Ding, K., Bi, J., et al. (2020). MgScH15: A Highly Stable Cluster for Hydrogen Storage. *Int. J. Hydrogen Energ.* 45, 32260–32268. doi:10.1016/j.ijhydene.2020.08.229

Frisch, M. J., Trucks, G. W., Schlegel, H. B., Scuseria, G. E., Robb, M. A., Cheeseman, J. R., et al. (2016). *Gaussian 09, Revision A.02*. Wallingford, CT: Gaussian, Inc. Available at: https://gaussian.com/g09citation/.

Huang, W., and Wang, L.-S. (2009). Probing the 2D to 3D Structural Transition in Gold Cluster Anions Using Argon Tagging. *Phys. Rev. Lett.* 102, 153401. doi:10.1103/PhysRevLett.102.153401

Idrobo, J. C., Walkosz, W., Yip, S. F., Öğüt, S., Wang, J., and Jellinek, J. (2007). Static Polarizabilities and Optical Absorption Spectra of Gold Clusters (Aun,n=2-14and 20) from First Principles. *Phys. Rev. B* 76, 205422. doi:10.1103/PhysRevB.76.205422

Jellinek, J., and Acioli, P. H. (2003). Magnesium Clusters: Structural and Electronic Properties and the Size-Induced Nonmetal-To-Metal Transition. *J. Phys. Chem. A.* 107, 1670. doi:10.1021/jp0301655

Jensen, F. (2017). *Introduction to Computational Chemistry*. West Sussex: John Wiley & Sons. Available at: https://xs.dailyheadlines.cc/books/about/Introduction_to_Computational_Chemistry.html?hl=zh-CN&id=UZOVDQAAQBAJ (Accessed October 14, 2021).

Jin, R. (2015). Atomically Precise Metal Nanoclusters: Stable Sizes and Optical Properties. *Nanoscale* 7, 1549–1565. doi:10.1039/C4NR05794E

Jin, R., Zeng, C., Zhou, M., and Chen, Y. (2016). Atomically Precise Colloidal Metal Nanoclusters and Nanoparticles: Fundamentals and Opportunities. *Chem. Rev.* 116, 10346–10413. doi:10.1021/acs.chemrev.5b00703

Köhn, A., Weigend, F., and Ahlrichs, R. (2001). Theoretical Study on Clusters of Magnesium. *Phys. Chem. Chem. Phys.* 3, 711–719. doi:10.1039/B007869G

Li, Z., Zhao, Z., Zhou, Z., Wang, H., and Li, S. (2017). First-principles Calculations on Small MgnZn and Mgn-1Zn2 Clusters: Structures, Stability, Electronic Properties. *Mater. Chem. Phys.* 199, 585–590. doi:10.1016/j.matchemphys.2017.07.049

Lu, C., and Chen, C. (2021). Indentation Strengths of Zirconium Diboride: Intrinsic versus Extrinsic Mechanisms. *J. Phys. Chem. Lett.* 12, 2848–2853. doi:10.1021/acs.jpclett.1c00434

Lu, C., and Chen, C. (2020a). Indentation-strain Stiffening in Tungsten Nitrides: Mechanisms and Implications. *Phys. Rev. Mater.* 4, 043402. doi:10.1103/PhysRevMaterials.4.043402

Lu, C., and Chen, C. (2020b). Structure-strength Relations of Distinct Mon Phases from First-Principles Calculations. *Phys. Rev. Mater.* 4, 044002. doi:10.1103/PhysRevMaterials.4.044002

Lu, C., Gong, W., Li, Q., and Chen, C. (2020). Elucidating Stress-Strain Relations of ZrB12 from First-Principles Studies. *J. Phys. Chem. Lett.* 11, 9165–9170. doi:10.1021/acs.jpclett.0c02656

Lu, T., and Chen, F. (2012). Multiwfn: A Multifunctional Wavefunction Analyzer. *J. Comput. Chem.* 33, 580–592. doi:10.1002/jcc.22885

Lv, J., Wang, Y., Zhu, L., and Ma, Y. (2012). Particle-swarm Structure Prediction on Clusters. *J. Chem. Phys.* 137, 084104. doi:10.1063/1.4746757

Lyon, J. T. (2021). Hydrogen Binding and Dissociation in MgScH Clusters (N ≤ 20). *Int. J. Hydrogen Energ.* 46, 36872–36877. doi:10.1016/j.ijhydene.2021.08.228

Peng, Y., Wang, P., Luo, L., Liu, L., and Wang, F. (2018). Green Synthesis of Fluorescent Palladium Nanoclusters. *Materials* 11, 191. doi:10.3390/ma11020191

Qian, H., and Jin, R. (2009). Controlling Nanoparticles with Atomic Precision: The Case of Au144(SCH2CH2Ph)60. *Nano Lett.* 9, 4083–4087. doi:10.1021/nl902300y

Ramakrishna, G., Varnavski, O., Kim, J., Lee, D., and Goodson, T. (2008). Quantum-Sized Gold Clusters as Efficient Two-Photon Absorbers. *J. Am. Chem. Soc.* 130, 5032–5033. doi:10.1021/ja800341v

Reed, A. E., Curtiss, L. A., and Weinhold, F. (1988). Intermolecular Interactions from a Natural Bond Orbital, Donor-Acceptor Viewpoint. *Chem. Rev.* 88, 899–926. doi:10.1021/cr00088a005

Shang, L., Dong, S., and Nienhaus, G. U. (2011). Ultra-small Fluorescent Metal Nanoclusters: Synthesis and Biological Applications. *Nano Today* 6, 401–418. doi:10.1016/j.nantod.2011.06.004

Shao, H., Xin, G., Zheng, J., Li, X., and Akiba, E. (2012). Nanotechnology in Mg-Based Materials for Hydrogen Storage. *Nano Energy* 1, 590–601. doi:10.1016/j.nanoen.2012.05.005

Shinde, R. (2016). Ab Initio Calculations of Optical Properties of Clusters. ArXiv160706928 Phys Available at: http://arxiv.org/abs/1607.06928 (Accessed October 11, 2021).

Shinde, R., and Shukla, A. (2017). First Principles Electron-Correlated Calculations of Optical Absorption in Magnesium Clusters. *Eur. Phys. J. D* 71, 301. doi:10.1140/epjd/e2017-80356-6

Sun, W., Kuang, X., Keen, H. D. J., Lu, C., and Hermann, A. (2020). Second Group of High-Pressure High-Temperature Lanthanide Polyhydride Superconductors. *Phys. Rev. B* 102, 144524. doi:10.1103/PhysRevB.102.144524

Tew, L., Cai, M.-T., Lo, L.-W., Khung, Y., and Chen, N.-T. (2018). Pollen-Structured Gold Nanoclusters for X-ray Induced Photodynamic Therapy. *Materials* 11, 1170. doi:10.3390/ma11071170

Trivedi, R., and Bandyopadhyay, D. (2015). Hydrogen Storage in Small Size MgnCo Clusters: A Density Functional Study. *Int. J. Hydrogen Energ.* 40, 12727–12735. doi:10.1016/j.ijhydene.2015.07.122

Trivedi, R., and Bandyopadhyay, D. (2016). Study of Adsorption and Dissociation Pathway of H 2 Molecule on Mg N Rh (N = 1-10) Clusters: A First Principle Investigation. *Int. J. Hydrogen Energ.* 41, 20113–20121. doi:10.1016/j.ijhydene.2016.09.007

Wang, Y., Lv, J., Zhu, L., and Ma, Y. (2012). CALYPSO: A Method for crystal Structure Prediction. *Comput. Phys. Commun.* 183, 2063–2070. doi:10.1016/j.cpc.2012.05.008

Wang, Y., Lv, J., Zhu, L., and Ma, Y. (2010). Crystal Structure Prediction via Particle-Swarm Optimization. *Phys. Rev. B* 82, 094116. doi:10.1103/PhysRevB.82.094116

Xia, X., Kuang, X., Lu, C., Jin, Y., Xing, X., Merino, G., et al. (2016). Deciphering the Structural Evolution and Electronic Properties of Magnesium Clusters: An Aromatic Homonuclear Metal Mg17 Cluster. *J. Phys. Chem. A.* 120, 7947–7954. doi:10.1021/acs.jpca.6b07322

Yan, N., Xia, N., Liao, L., Zhu, M., Jin, F., Jin, R., et al. (2018). Unraveling the Long-Pursued Au 144 Structure by X-ray Crystallography. *Sci. Adv.* 4, eaat7259. doi:10.1126/sciadv.aat7259

Yau, S. H., Varnavski, O., and Goodson, T. (2013). An Ultrafast Look at Au Nanoclusters. *Acc. Chem. Res.* 46, 1506–1516. doi:10.1021/ar300280w

Zeng, L., Liang, M.-K., Wei, X.-F., Guo, J., Dai, W., and Zhu, B.-C. (2021). New Potential Stable Structures of XMg N (X = Ge, C, Sn; N = 2-12) Clusters: XMg8 with High Stability. *J. Phys. Condens. Matter* 33, 065302. doi:10.1088/1361-648X/abc401

Zeng, L., Wei, X.-F., Liang, M.-K., Deng, P.-J., Bi, J., and Zhu, B.-C. (2020). BeMg9: A tower-like Type Doped Magnesium Clusters with High Stability. *Comput. Mater. Sci.* 182, 109795. doi:10.1016/j.commatsci.2020.109795

Zhang, F., Zhang, H., Xin, W., Chen, P., Hu, Y., Zhang, X., et al. (2020). Probing the Structural Evolution and Electronic Properties of Divalent Metal Be2Mgn Clusters from Small to Medium-Size. *Sci. Rep.* 10, 6052. doi:10.1038/s41598-020-63237-8

Zhao, Y. R., Bai, T. T., Jia, L. N., Xin, W., Hu, Y. F., Zheng, X. S., et al. (2019). Probing the Structural and Electronic Properties of Neutral and Anionic Lanthanum-Doped Silicon Clusters. *J. Phys. Chem. C* 123, 28561–28568. doi:10.1021/acs.jpcc.9b07184

Zhao, Y., Xu, Y., Chen, P., Yuan, Y., Qian, Y., and Li, Q. (2021). Structural and Electronic Properties of Medium-Sized Beryllium Doped Magnesium BeMg Clusters and Their Anions. *Results Phys.* 26, 104341. doi:10.1016/j.rinp.2021.104341

Zhu, B.-C., Deng, P.-J., Xiong, S.-Y., Dai, W., Zeng, L., and Guo, J. (2021). Au5Br: A New Member of Highly Stable 2D-type Doped Gold Nanomaterial. *Comput. Mater. Sci.* 194, 110446. doi:10.1016/j.commatsci.2021.110446

Zhu, B. C., Zhang, S., and Zeng, L. (2020). The Effect of Silicon Doping on the Geometrical Structures, Stability, and Electronic and Spectral Properties of Magnesium Clusters: DFT Study of SiMg N (N = 1-12) Clusters. *Int. J. Quan. Chem.* 120, e26143. doi:10.1002/qua.26143

Conflict of Interest: The authors declare that the research was conducted in the absence of any commercial or financial relationships that could be construed as a potential conflict of interest.

Publisher's Note: All claims expressed in this article are solely those of the authors and do not necessarily represent those of their affiliated organizations, or those of the publisher, the editors and the reviewers. Any product that may be evaluated in this article, or claim that may be made by its manufacturer, is not guaranteed or endorsed by the publisher.